Antibacterial activity and biofilm inhibition by surface modified titanium alloy medical implants following application of silver, titanium dioxide and hydroxyapatite nanocoatings

NANOTOXICOLOGY, 2017
VOL. 11, NO. 3, 327–338
http://dx.doi.org/10.1080/17435390.2017.1299890

Taylor & Francis
Taylor & Francis Group

ORIGINAL ARTICLE

OPEN ACCESS Check for updates

Antibacterial activity and biofilm inhibition by surface modified titanium alloy medical implants following application of silver, titanium dioxide and hydroxyapatite nanocoatings

A. Besinis[a,b,c], S. D. Hadi[a], H. R. Le[c], C. Tredwin[b] and R. D. Handy[a]

[a]School of Biological Sciences, University of Plymouth, Plymouth, UK; [b]Plymouth University Peninsula Schools of Medicine and Dentistry, University of Plymouth, Plymouth, UK; [c]School of Engineering, University of Plymouth, Plymouth, UK

ABSTRACT

One of the most common causes of implant failure is peri-implantitis, which is caused by bacterial biofilm formation on the surfaces of dental implants. Modification of the surface nanotopography has been suggested to affect bacterial adherence to implants. Silver nanoparticles are also known for their antibacterial properties. In this study, titanium alloy implants were surface modified following silver plating, anodisation and sintering techniques to create a combination of silver, titanium dioxide and hydroxyapatite (HA) nanocoatings. Their antibacterial performance was quantitatively assessed by measuring the growth of *Streptococcus sanguinis*, proportion of live/dead cells and lactate production by the microbes over 24 h. Application of a dual layered silver–HA nanocoating to the surface of implants successfully inhibited bacterial growth in the surrounding media (100% mortality), whereas the formation of bacterial biofilm on the implant surfaces was reduced by 97.5%. Uncoated controls and titanium dioxide nanocoatings showed no antibacterial effect. Both silver and HA nanocoatings were found to be very stable in biological fluids with material loss, as a result of dissolution, to be less than 0.07% for the silver nanocoatings after 24 h in a modified Krebs-Ringer bicarbonate buffer. No dissolution was detected for the HA nanocoatings. Thus, application of a dual layered silver–HA nanocoating to titanium alloy implants creates a surface with antibiofilm properties without compromising the HA biocompatibility required for successful osseointegration and accelerated bone healing.

ARTICLE HISTORY
Received 11 August 2016
Revised 26 January 2017
Accepted 21 February 2017

KEYWORDS
Biomaterials; nanotopography; nanoparticles; medical microbiology; nanosurfaces

Introduction

The success of a dental implant is determined by the inflammatory response and the behaviour of the adjacent tissues at the tissue-implant interface. Titanium and its alloys (e.g., Ti6Al4V) are the most common materials employed for manufacturing medical and dental implants due to their good biocompatibility, mechanical strength and corrosion resistance (Norowski & Bumgardner, 2009; Williams, 1977). Despite the high success rates of dental implants, 5–10% of them are still reported to fail mainly due to mechanical problems, poor osseointegration, infection, or rejection (Moy et al., 2005); and must be removed. Among these causes, the development of peri-implantitis remains the main reason for implant failure (Paquette et al., 2006). The survival of pathogenic microbes in the oral cavity depends on their ability to successfully develop into biofilms, which protects them from environmental challenges and enhances their growth (Dunne, 2002). Biofilm formation on the surfaces of dental implants is one of the main causes of peri-implantitis (Zhao et al., 2009).

Strategies to render the surface of dental implants antibacterial with the aim to prevent infection and peri-implantitis development include application of antimicrobial coatings loaded with antibiotics (Alt et al., 2006) or chlorhexidine (Kozlovsky et al., 2006). However, such approaches usually suffer from short-term antimicrobial efficacy (Radin et al., 1997), whereas the use of chlorhexidine has also been reported to have a cytotoxic effect on human cells (Lessa et al., 2010; Pucher & Daniel, 1992). The addition of zinc to magnesium alloy biodegradable implants has been found to offer antibacterial protection without compromising biocompatibility (He et al., 2015). Similarly, a composite nanocoating was synthesised by embedding silver nanoparticles (Ag NPs), known to have an intrinsic antibacterial activity, with bioactive glass in a polymer matrix of polyetheretherketone to render the surfaces of implants both antibacterial and biocompatible (Seuss et al., 2016). In a recent study, Mishra et al. (2016) developed a hybrid nanocoating for titanium implants in an attempt to combine the antibacterial effect of Ag NPs with sustained drug delivery. The coating consisted of Ag NPs cored inside polyvinyl alcohol nanocapsules, both embedded in a chitosan matrix loaded with the anti-inflammatory drug naproxen.

Metal NPs especially have been successfully employed in dental applications offering infection control and management of the oral biofilm (Allaker, 2010). The precise mechanism(s) of antibacterial action of metal NPs is still not fully understood, but possibilities include free metal ion toxicity due to dissolution of the particle surface (e.g., Ag^{+} from Ag NPs, Kim et al., 2007). The resulting metal ions may inhibit enzyme activity in microbes including the respiratory chain, as well as proteins on the bacterial cell membrane (Morones et al., 2005). Some metals can also initiate oxidative stress by the direct generation of reactive oxygen

CONTACT Alexandros Besinis alexander.besinis@plymouth.ac.uk, abessinis@hotmail.com School of Engineering, University of Plymouth, Drake Circus, Plymouth PL4 8AA, UK

species (ROS). The latter mechanism of injury to microbes is particular important for anatase forms of TiO_2, where ROS are produced following photocatalysis of the TiO_2 particle surface with water (Hirakawa et al., 2004; Wong et al., 2006). However, Ag NPs are arguably the most antibacterial against oral pathogens compared to other metal NPs and nano-particulate metal oxides (Besinis et al., 2014a; Vargas-Reus et al., 2012).

The application of a thin ceramic layer on metallic implants is known to enhance osseointegration, osteogenesis and inhibit adverse inflammatory reactions (Phillips et al., 2003; We et al., 2005). The ceramic nanomaterials used as coatings on the surface of titanium implants need to be biocompatible and biomimetic; with bioactive glass, calcium hydroxyapatite (HA) and other calcium phosphate compounds being commonly used (Besinis et al., 2015). Synthetic nano-hydroxyapatite (nHA) is a preferable material because it is chemically and biologically similar to the natural mineral component of bone and teeth. Thus, it is used routinely in orthopaedic, dental and maxillofacial applications (Figueiredo et al., 2010). Previous *in vivo* studies have reported that titanium dental implants whose surface has been modified with HA NPs performed better compared to their uncoated controls; demonstrating an enhanced bone-to-implant contact and accelerated formation of new bone (Svanborg et al., 2011; Yang et al., 2009).

Ideally, the dental implants should have materials that impart both biocompatible and antimicrobial properties. This can be achieved with a composite material. The hypothesis of this study was that creating Ti6Al4V medical implants whose surfaces have been modified with a combination of TiO_2, Ag and HA NPs will provide a biocompatible surface that also has antibacterial and antibiofilm properties. The antimicrobial properties of the different nanomaterials and nanocoatings under investigation were tested against one of the most common pathogens associated with peri-implantitis and dental implant infections, *Streptococcus sanguinis*. The second objective was to examine the stability of the coatings and their ability to maintain their integrity in biological fluids. Finally, the factors that may determine their antibacterial behaviour, such as particle chemistry, particle morphology and surface nanotopography, were also investigated.

Methods and materials

Preparation of titanium discs

Round titanium discs, having a diameter of 15 mm and thickness of 1 mm, were laser cut from a medical quality titanium alloy Ti6Al4V (ASTM Grade 5) sheet. The titanium discs were polished with progressively finer grades of silicon carbide abrasive paper (P800 and P1200) using a rotary grinding and polishing device (Grinder-Polisher, Buehler UK Ltd, Coventry, UK) for 10 min. The final polishing was achieved using a 1 μm diamond paste (Kemet International Ltd, Kent, UK). The discs were cleaned for 5 min in an ultrasonic bath (Metason 120 T, power supply 125 W, HF-output power 70 W, Struers, Rotherham, UK) using a 20 g l^{-1} NaOH and Na_2CO_3 solution, followed by immersing the discs in a 5% HCl solution for another 5 min to remove the oxide layer from the surface of the discs.

Surface modification of titanium discs

After being polished and cleaned, the titanium discs were coated with TiO_2 NPs and Ag NPs following anodisation and electroplating techniques, respectively, whereas titanium discs were coated with nHA and micro-HA (mHA) particles using a sintering technique. In total, nine different groups were prepared ($n = 9$ discs/treatment): uncoated Ti6Al4V control discs (Ti), Ti6Al4V discs coated with nHA (Ti + nHA), Ti6Al4V discs coated with mHA (Ti + mHA), anodised Ti6Al4V discs (TiO_2), anodised Ti6Al4V discs coated with nHA (TiO_2+nHA), anodised Ti6Al4V discs coated with mHA (TiO_2+mHA), silver plated Ti6Al4V discs (Ag), silver plated Ti6Al4V discs coated with nHA (Ag + nHA) and silver plated Ti6Al4V discs coated with mHA (Ag + mHA).

Electroplating technique (nano-silver coating)

The Ti6Al4V discs, where appropriate, were coated with Ag NPs by electroplating according to the method described by Sieh et al. (2015). Each time, a disc was connected to the end of a silver wire (cathode), whereas a second silver wire (anode) was the silver source. The ends of both wires (including the titanium disc) were immersed in a silver solution (electrolyte) consisting of 0.2 M Ag, 0.4 M succinimide and 0.5 M KOH (pH 8.5). The other ends of the silver wires (anode and cathode) were connected to a DC power supply accordingly. The voltage was adjusted to 1 V and the current to 0.1 A. The electrolyte was heated to 40 °C to increase the adhesion of silver to the surface of the titanium discs and the electroplating time was 3 min. The electroplated titanium discs were rinsed with distilled water and left to air-dry. A small pilot study was also conducted in order to estimate the amount of silver on a representative batch of discs. The approach was to aggressively clean the discs of any attached silver with strong nitric acid. Briefly, ultrasonic cleaning was performed with discs placed in glass vials containing 6 ml of 15% nitric acid in saline for 2 h. The resulting solution was analysed for total silver content (see below).

Anodisation technique (titanium dioxide nanocoating)

The anodisation technique was used to create a dense nano-particulate, compact and thin oxide layer on the surface of titanium discs, where appropriate to the treatment. Each time, a titanium disc was connected to the end of a platinum wire (anode) and a copper plate was used as the counter electrode (cathode). One end of the platinum wire (including the titanium disc) and the copper plate were immersed in the electrolyte solution (5 g l^{-1} sodium acetate). A DC power supply was used to apply the anodisation voltage (30 V for 5 min). The anodised discs were rinsed with distilled water and left to air-dry.

Sintering technique (nano-HA and micro-HA coatings)

Where required, the Ti6Al4V discs were fully and evenly coated with nHA (particle size: 25.96 ± 8.42 nm in length and 13.60 ± 2.56 nm in width; nanoXIM-HAp102, Fluidinova SA, Moreira da Maia, Portugal) and mHA particles (particle size: 4.72 ± 2.29 μm; nanoXIM-HAp202, Fluidinova SA, Moreira da Maia, Portugal) by introducing 20 μl of a nHA or mHA solution, respectively, to the upper surface of each disc. The solutions consisted of 15% (w/v) nHA or mHA powder in Milli-Q ultra-pure water. The coated discs were left to dry at room temperature for 48 h and then placed in a furnace (ELF 11/14, Carbolite Ltd, Hope Valley, UK) to sinter the HA particles in order to improve stability of the coatings and increase adhesion on the Ti6Al4V surface. The heating rate was 10 °C min^{-1} and the sintering temperature was 500 °C. The holding time at sintering temperature was 10 min followed by slow furnace cooling to room temperature.

Surface characterisation of titanium discs

Surface topography, especially surface roughness can be an important modulating factor in the initial formation of biofilms. The surface roughness was quantified by measuring the arithmetical mean deviation of the roughness profile (Ra) and the

maximum primary height of roughness profile (Rz) using an Olympus LEXT OLS 3000 confocal laser scanning microscope equipped with a 408 nm LD class 2 laser. The measurements were performed using a total magnification of 50× and an optical zoom of 1×. Profiles were Gaussian filtered with a cut-off wavelength value of 85.2 μm. Surface roughness was measured at three different locations on the surface of each disc ($n = 3$ discs/treatment). The fine-scale surface nanotopography of the coated discs was further investigated by 3D analysis using the Olympus LEXT OLS 6.0.7 software.

The surface morphology of the control and coated discs was examined using scanning electron microscopy (SEM), whereas energy dispersive X-ray spectroscopy (EDS) was employed to analyse the elemental composition of the specimens' surface and to confirm that the application of the coatings was successful ($n = 3$ discs/treatment). Specimens were analysed with a JEOL7001F field emission scanning electron microscope (FESEM) equipped with Oxford Instruments AZtec X-Ray analysis system. Specimens did not require to be sputter coated prior to analysis as their surfaces were electrically conducting. Identical operating conditions and scanning parameter settings were used for all EDS scans (spot size: 10; accelerating voltage: 15 kV; working distance 10 mm). Data and spectra analyses were achieved using Aztec 2.2 software (Oxford Instruments, Abingdon, UK).

Experimental design and preparation of microplates

The experimental design involved exposing *S. sanguinis* in 24-well microplates (flat-bottom sterile polystyrene microplates, Nunc, Thermo Fischer Scientific, Loughborough, UK) for 24 h to the coated Ti6Al4V discs ($n = 6$/treatment) in comparison to the uncoated control discs (negative control) and blank controls (no disc in the well). *S. sanguinis* was selected as the most common pathogen causing peri-implantitis and dental implant infections. The 24-well microplate was used as the unit of replication ($n = 6$ plates/treatment) with at least two different batches of cells. The study design was achieved after pilot studies explored within and between plate variation and the best way to apply the coatings (data not shown). Cultures of *S. sanguinis* (NCTC 10904) were grown in Brain Heart Infusion (BHI, product code: OXCM1135B, Fisher Scientific, Loughborough, UK) broth supplemented with 2% sucrose. Each Ti6Al4V disc was placed on the bottom of a well with the coated surface facing upwards. All discs had been previously gamma radiated (36.42–40.72 kGy, 10 h) to ensure sterility. Each well was inoculated with 150 μl of bacterial suspension (10^7 CFU ml^{-1}) and 1.5 ml of sterile physiological saline (modified Krebs-Ringer bicarbonate buffer consisting of 118 mM NaCl, 3 mM KCl, 1 mM $MgSO_4 \cdot 5H_2O$, 2 mM $CaCl_2$, 25 mM $NaHCO_3$, 1.2 mM KH_2PO_4 and 10 mM glucose) was added. The microplates were then incubated for 24 h at 37 °C under 5% CO_2 in atmospheric air to allow bacterial growth. At the end of the exposure, the bacteria in the media were assessed for bacterial growth, cell viability and lactate production following the protocols previously described by Besinis et al. (2014a). Briefly, bacterial growth was assessed by reading the turbidity values at 595 nm (VersaMax microplate reader with SoftMax Pro 4.0 software, Molecular Devices, Sunnyvale, CA) with corrections for the background turbidity of the media. The antibacterial activity of the coatings was also assessed by measuring the proportion of live and dead cells, and lactate production (see below). The total Ag, Ti, P and Ca concentrations in the media were measured by inductively coupled plasma mass spectrometry (ICP-MS, X Series 2, Thermo Scientific, Hemel Hempstead, UK) to investigate the stability of the coatings and aid interpretation of the data. Both nHA and mHA coatings consisted of calcium hydroxyapatite [$Ca_{10}(PO_4)_6(OH)_2$] and therefore phosphorous (P) and calcium (Ca) were selected to identify potential dissolution or degradation of the HA coatings. The method used matrix matched standards (physiological saline/BHI broth in 10:1 ratio). At the end of the 24 h exposure, Ti6Al4V discs were removed from the microplates to assess the biofilm development on the specimens (see below).

Assessment of bacteria viability

The viability of *S. sanguinis* suspended in the media after 24 h exposure was assessed using the L7012 Live/Dead® Backlight™ Kit (Invitrogen Ltd, Paisley, UK). The manufacturer's protocol was used but with optimised emission wavelengths as described by Besinis et al. (2014a). The kit consists of two stains, SYTO 9 which is a green fluorescent DNA stain for all kinds of cells, and propidium iodide, a red fluorescent DNA stain for cells with a compromised membrane. The staining solution was prepared by mixing the two stains provided at a 1:1 ratio and then adding Milli-Q ultra-pure water to a final total stain concentration of 0.6%. The cell viability was measured by transferring 100 μl of media from each well/container to a 96-well plate (flat-bottom sterile polystyrene microplates, FB56416, Fisherbrand, Loughborough, UK) and mixing thoroughly with an equal volume of the staining solution. The 96-well microplates were then incubated at room temperature in the dark for 15 min. The samples were examined immediately using a Cytofluor II fluorescence plate reader (Perspectives Biosystems, Framingham, MA). The emission wavelengths were set at 530 for SYTO 9 and 645 nm for propidium iodide, whereas the excitation wavelength was 480 nm for both dyes. The kit was calibrated as previously described by Besinis et al. (2014a) so the experimental fluorescence data obtained were converted to an equivalent percentage of live bacteria.

Determination of the lactate production

The amount of lactate that was produced by *S. sanguinis* was measured using the lactate production assay, as an indicator of the presence of metabolically active bacterial cells (Besinis et al., 2014a). After 24 h incubation of the microplates, 100 μl from each well were transferred to V-bottom 96-well microplates (product number: 3896, Corning, Deeside, UK) which were then centrifuged (2000 rpm for 20 min with a 2040 Rotors microplate centrifuge, Centurion Scientific Ltd, Ford, UK) to pellet the bacteria. Then, 10 μl of the supernatant from each well were carefully transferred to flat bottom 96-well microplates and mixed with 211 μl of a lactate assay reagent according to Gutmann and Wahlefeld (1974). The lactate assay reagent consisted of 200 μl of hydrazine–glycine buffer (0.4 M hydrazine and 0.5 M glycine solution buffered to pH 9 with KOH), 10 μl of 40 mM nicotinamide adenine dinucleotide (NAD^+, Melford Laboratories Ltd, Suffolk, UK) and 1 μl of 1000 units ml^{-1} lactate dehydrogenase (LDH, Sigma-Aldrich Ltd, Poole, UK). Samples were incubated for 2 h at 37 °C and absorbances were read with the VersaMax plate reader at 340 nm. Absorbances were converted to molar concentration using a calibration curve of lactic acid standards in triplicates (0, 0.125, 0.25, 0.5, 1.0, 2.0, 4.0, 8.0 and 16 mM).

Assessment of bacterial adhesion

The viability of the bacteria adhered to the control and coated Ti6Al4V discs was assessed by following the protocol described by Besinis et al. (2014b) with some modifications. In brief, all discs ($n = 6$/treatment) were aseptically removed from the 24-well

microplates at the end of the 24 h exposure and rinsed three times with sterile saline (0.85% NaCl) to remove the non-adherent bacteria. Each disc was then placed in a separate sterile glass vial containing 2 ml of sterile saline and sonicated in an ultrasonic bath (35 kHz frequency, Fisherbrand FB 11010, Schwerte, Germany) for 60 s to detach the bacteria adherent to the disc surfaces and bring them in suspension. Afterwards, the discs were removed and the solutions were vortexed for 3 s. Then, 0.5 ml of the media from the sonicated discs was added to 5 ml of BHI +2% sucrose broth and incubated for 16 h at 37 °C under 5% CO_2 in atmospheric air. At the end of the 16 h incubation, the turbidimetric values were recorded to assess the bacterial adhesion using a VersaMax microplate reader at 595 nm (Molecular Devices, Sunnyvale, CA), according to Besinis et al. (2014a). For a relative measurement of bacterial adhesion, the turbidity values of each test sample were expressed in comparison to the mean value of the uncoated controls corresponding to 100% of bacterial adhesion. The percentage of live bacteria and their lactate production were also measured after 16 h of incubation following the same protocols as described above.

Twenty seven additional discs ($n = 3$/treatment) were used to investigate the bacterial adhesion on the uncoated controls compared to the test coated surfaces by means of SEM. This required a different SEM specimen preparation technique to preserve the biofilm compared to that used to examine the surface morphology of the manufactured control and coated discs above. At the end of the 24 h exposure, the specimens were removed from the 24-well microplates and rinsed three times with sterile saline to remove the non-adherent bacteria. Then, specimens were fixed overnight at 4 °C with 3% glutaraldehyde in 0.1 M cacodylate buffer. Fixed specimens were rinsed (3 × 3 min) with 0.1 M cacodylate buffer to remove glutaraldehyde and subsequently dehydrated with ascending ethanol steps and hexamethyldisilazane (HMDS). Specimens were finally chromium sputtered prior to analysis with the JEOL7001F FESEM.

Statistics

All data are presented as means ± SEM and were analysed using the IBM SPSS Statistics version 22.0 for Windows (SPSS Inc., Chicago, IL). The differences between the coated test specimens and the uncoated controls or blanks (treatment effect) were evaluated using one-way analysis of variance (one-way ANOVA, Tukey's post hoc test) for each method/variable. All statistical analysis used a 95% confidence limit, so that p values equal to or greater than 0.05 were not considered statistically significant.

Results

Surface characterisation of titanium discs

Prior to assessing the antibacterial and antibiofilm properties of the nanocoatings applied to the Ti6Al4V discs, SEM images were obtained to verify the surface morphology of the specimens before the start of experiments (Figure 1). The SEM analysis confirmed that application of the nano-silver, nHA and mHA coatings was successful with images showing the presence of even and continuous layers of particles covering the surface of all Ti6Al4V discs (Figure 1(A–H)). The only exception was the mHA coating applied to the silver plated discs, where some small gaps were visible revealing the underlying silver nanocoating (Figure 1(I)). Further analysis with EDS confirmed the presence of the nanocoatings and their elemental composition. Quantitative analysis of the control Ti6Al4V discs showed that the weight percentages of titanium, aluminium and vanadium (89.5, 6.0 and 2.5%, respectively) were as expected, while also lacking oxygen. The anodised discs contained 14% of oxygen due to the formation of the oxide layer following oxidisation, whereas the surface of the silver plated discs consisted of 24% nano-silver (Figure 1).

The surface roughness measurements are shown in Table 1. Anodisation or silver plating of the Ti6Al4V discs had no significant effect on the surface roughness of the specimens ($p > 0.05$). Application of the nHA coating to the Ti, TiO_2 and Ag discs did not result in statistically higher Ra surface roughness values ($p > 0.05$), except for the TiO_2+nHA specimens compared to the TiO_2 discs ($p < 0.01$). However, application of the mHA coating caused a significant increase in the surface roughness (Ra) of the specimens ($p < 0.001$). There was also a significant difference between the mHA coated specimens and those coated with nHA ($p < 0.001$), with the exception of the Ti + mHA discs ($p > 0.05$). Further 3D analysis of the surface morphology of the discs confirmed those findings with the images acquired showing an apparent increase in the surface roughness of the specimens coated with nHA and mHA particles (Figure 2).

Stability of the antibacterial coatings

The stability of the silver nanocoatings was assessed by measuring the total concentration of silver in the media at the end of the 24 h exposure and also after mild sonication of the samples for 60 s which was used to remove the biofilm from the discs. The ICP-MS measurements were also performed for Ti, P and Ca to determine the dissolution of titanium from the control and anodised Ti6Al4V discs, and assess the stability of the two HA coatings accordingly (Table 2).

Silver

The pilot study using aggressive ultrasonic cleaning in 15% nitric acid for 2 h in order to remove all the silver from the surface of a new disc showed that the total amount of silver present on each silver plated disc was 0.9 mg. In theory for the subsequent biological experiments, if all the silver was dissolved or dislodged from the silver nanocoating at the end of the 24 h incubation, this would equate to a maximum silver concentration of 548 mg l^{-1} in the media in each microplate well. At the end of the experiment, a more gentle sonication was also used to detach the biofilm from the disc surfaces into saline contained in glass vials so that biochemical analysis could be performed. For these samples, in theory if all of the silver had detached or dissolved (unlikely with the mild sonication used, unlike the aggressive nitric acid cleaning above), a maximum of 452 mg l^{-1} of silver would be present in the saline in each glass vial along with the detached bacteria. The measured silver concentrations were found to be considerably lower in physiological saline at the end of the 24 h incubation period ($\leq$0.34 mg l^{-1} or <0.07% of the total silver present on discs) confirming a limited dissolution of silver from the nanocoatings to the media during the experiments. Nevertheless, at the end of the experiment, the silver release from the silver plated discs that were additionally coated with nHA or mHA particles (0.34 ± 0.01 and 0.32 ± 0.01 mg l^{-1} for the Ag + nHA and Ag + mHA discs, respectively, $n = 6$) was two-fold higher compared to that of the Ag discs (0.16 ± 0.01 mg l^{-1}), with the difference being statistically significant ($p < 0.05$). Analysis of the media after sonication of the silver plated discs for 60 s to remove the bacteria also demonstrated low metal concentrations (0.83 ± 0.05, 1.05 ± 0.13 and

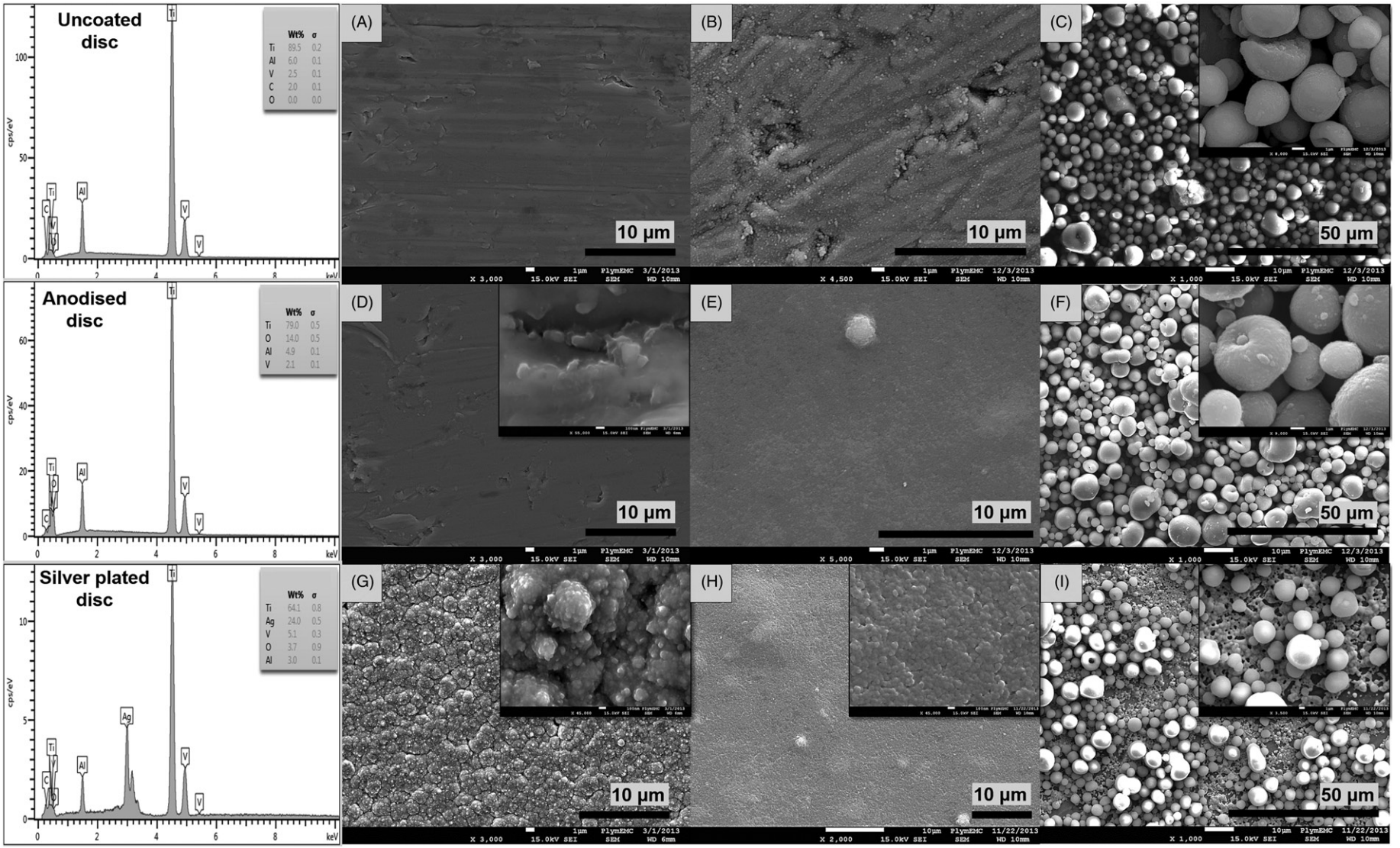

Figure 1. Scanning electron micrographs showing the surface morphology of (A) uncoated Ti6Al4V control discs (3.0k), (B) Ti6Al4V discs coated with nHA (×4.5k), (C) Ti6Al4V discs coated with mHA (×1.0k), (D) anodised Ti6Al4V discs (×3.0k), (E) anodised Ti6Al4V discs coated with nHA (×5.0k), (F) anodised Ti6Al4V discs coated with mHA (×1.0k), (G) Ti6Al4V discs coated with nano-silver (×3.0k), (H) Ti6Al4V discs coated with nano-silver and nHA (×2.0k) and (I) Ti6Al4V discs coated with nano-silver and mHA (×1.0k). Additional SEM images shown in the top right corners demonstrate details of the surface nanotopography at higher magnification. The EDS spectra show the elemental composition of the uncoated, anodised and silver plated disc surfaces.

Table 1. Surface roughness values of the uncoated controls and coated test discs.

Type of nanocoating	Rz (μm)	Ra (μm)
Ti	12.274 ± 0.329^{a}	0.358 ± 0.011^{a}
Ti + nHA	21.888 ± 1.244^{bc}	0.977 ± 0.120^{ab}
Ti + mHA	27.293 ± 1.531^{d}	1.562 ± 0.168^{bcd}
TiO_2	16.027 ± 0.973^{ae}	0.691 ± 0.057^{ae}
TiO_2+nHA	18.073 ± 0.877^{be}	1.710 ± 0.129^{cd}
TiO_2+mHA	26.693 ± 1.495^{cd}	3.012 ± 0.241^{f}
Ag	12.744 ± 0.485^{a}	0.796 ± 0.043^{ag}
Ag + nHA	24.591 ± 1.566^{cdf}	1.153 ± 0.131^{bceg}
Ag + mHA	20.886 ± 0.582^{bf}	2.241 ± 0.263^{d}

Measurements from three different sites on the surface of each disc ($n = 3$ discs/treatment) were taken (magnification 50×, optical zoom 1×). Data are expressed as mean ± SEM ($n = 9$) values. Different letters indicate significant differences between the test groups (one-way ANOVA, $p < 0.05$).

$0.13 \pm 0.03\ mg\ l^{-1}$ for the Ag, Ag + nHA and Ag + mHA discs, respectively).

Titanium

The release of titanium from the Ti6Al4V discs was found to be low at the end of the 24 h exposure. Concentration values did not exceed $0.03\ mg\ l^{-1}$ for all test groups except for the uncoated controls (Ti discs) where the concentration was $0.08\ mg\ l^{-1}$. Titanium release after disc sonication used to remove the biofilm was less than $0.32\ mg\ l^{-1}$. The Ti and Ag discs showed no titanium release, whereas the release from the TiO_2 discs was negligible ($\leq 0.01\ mg\ l^{-1}$). However, titanium concentrations in the sonicated media were a little higher for those discs that had been coated with nHA or mHA (concentration range: 0.05–$0.32\ mg\ l^{-1}$), with the differences being statistically significant compared to the Ti, TiO_2 and Ag discs ($p < 0.05$), but not the TiO_2+nHA discs ($p > 0.05$).

Hydroxyapatite

The phosphorous and calcium concentrations in the media (blank controls) were 104.72 ± 1.88 and $56.00 \pm 0.87\ mg\ l^{-1}$, respectively. The concentration of phosphorous in the media remained unchanged for all test groups regardless of the nanocoating. Results showed some calcium release to the media from the Ti + nHA and Ti + mHA discs, but the increase was not statistically significant ($p > 0.05$). The calcium concentration in the media was found to be lower for all the remaining groups when compared to the blank controls. Coating the discs with HA involved the application of 20 μl solutions containing 15% (w/v) nHA or mHA, which equates to 3 mg of HA material for each specimen (0.56 mg of phosphorous and 1.20 mg of calcium). If there was complete dissolution or degradation of the HA coatings due to sonication of the discs to remove the biofilm, the expected phosphorous and calcium concentrations would be 280 and $600\ mg\ l^{-1}$ respectively. Therefore, the 60 s disc sonication caused approximately 7% material loss of HA from the Ti + nHA and Ti + mHA discs, 1.2% from the TiO_2+nHA and TiO_2+mHA discs, and 5% from the Ag + nHA and Ag + mHA discs.

Growth and viability of bacteria in suspension

All three bioassays clearly showed that the silver plated discs exhibited the highest antibacterial activity with anodised discs also demonstrating some antibacterial effect. The presence of the nHA and mHA coatings was found to increase the antibacterial performance of the specimens further (Figure 3(A,C,E)).

The antibacterial activity of the Ti6Al4V disc nanocoatings against *S. sanguinis* was initially investigated by turbidity measurements to indicate growth of the organism (Figure 3(A)). Application of the nHA and mHA coatings on the surface of the Ti6Al4V discs (Ti + nHA and Ti + mHA specimens) significantly reduced the growth of bacteria suspended in the media compared to the uncoated controls ($p < 0.001$). The TiO_2, TiO_2+nHA and TiO_2+mHA discs also showed significant antibacterial activity ($p < 0.01$) although their performance was similar to that of the Ti + nHA and Ti + mHA discs ($p > 0.05$). The silver plated discs further inhibited bacterial growth in the media with turbidity values being at least three-fold lower compared to the anodised groups. The Ag + nHA and Ag + mHA discs demonstrated the strongest antibacterial activity ($p < 0.05$ compared to Ag discs and $p < 0.001$ for all remaining groups) where complete inhibition of bacterial growth was achieved.

The Live/Dead assay confirmed the strong antibacterial performance of the Ag, Ag + nHA and Ag + mHA discs with findings showing the absence of viable bacteria in the media at the end of the 24 h incubation (Figure 3(C)). Cell viability as a result of exposure to the anodised discs was not statistically different compared to the uncoated controls ($p > 0.05$). However, the presence of the additional nHA and mHA coatings on the surface of the anodised and uncoated discs caused significantly higher cell damage to suspended bacteria ($p < 0.05$) reducing the cell viability by 40% compared to the TiO_2 discs and 50% compared to the Ti discs.

The supremacy of the antibacterial activity of the Ag, Ag + nHA and Ag + mHA discs was further supported by the lactate production measurements (Figure 3(E)), with concentration values being significantly lower compared to all the remaining groups ($p < 0.001$). The lactate concentration for the silver plated discs was 0.09 ± 0.03 mM ($n = 6$), whereas no lactate was detected in the case of the Ag + nHA and Ag + mHA discs. The lactate production for the remaining groups ranged from 11.59 to 13.13 mM.

Antibiofilm activity

Examination of the discs at the end of the incubation period by SEM showed varying levels of biofilm development on the surface of the nanocoatings that were consistent with the growth and biochemical observations above. All the silver plated discs (Ag, Ag + nHA, Ag + mHA) had a strong antibiofilm activity as confirmed by the lack of biofilm development on the disc surfaces. Only a small number of scattered micro-organisms were detected with evident signs of limited cell division (Figure 4(G–I)). Application of the nHA and mHA coatings to the silver plated discs did not diminish their antibiofilm performance. All the remaining discs had no antibiofilm activity with their surfaces covered by a continuous biofilm formed by *S. sanguinis*, which in most cases was thicker than a monolayer (Figure 4(A–F)).

Quantitative results from the bioassays confirmed the findings of the SEM analysis of the biofilms. Bacterial adhesion on all the silver plated discs was significantly lower compared to the uncoated controls and the remaining test groups ($p < 0.001$). The highest biofilm inhibition was measured for the Ag + nHA discs with the mean adhesion value being just 2.5% of that exhibited by the uncoated controls, and followed by the Ag and Ag + mHA discs with adhesion values of 3.3 and 9.7%, respectively. There was no statistical difference between the three silver plated groups (Figure 3(B); $p > 0.05$). Adhesion values of the remaining groups were at least 91.1% suggesting the presence of a fully developed biofilm and thus no antibiofilm activity. The TiO_2, TiO_2+nHA and TiO_2+mHA discs were not statistically different compared to the uncoated controls ($p > 0.05$), whereas the

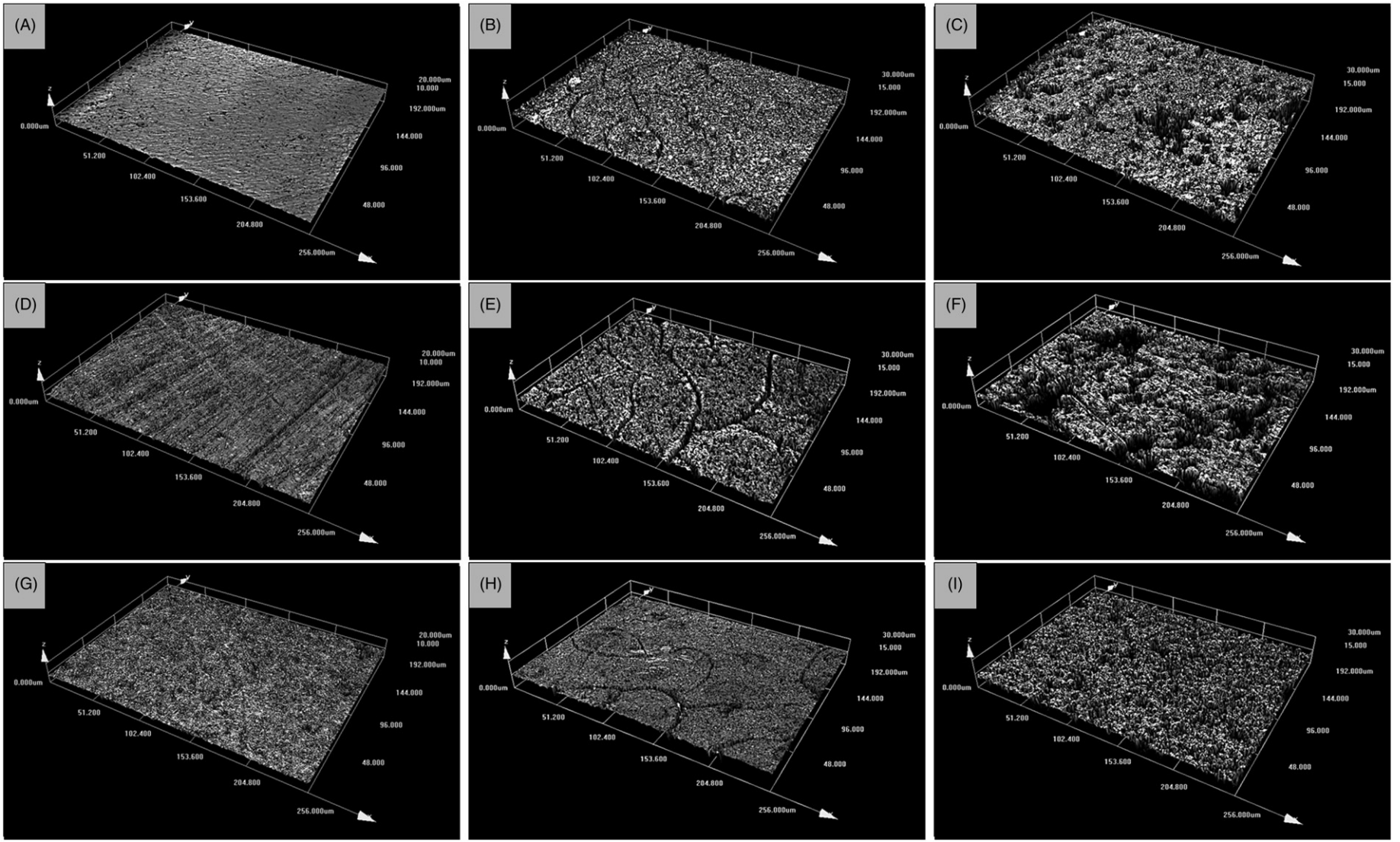

Figure 2. Example three-dimensional images showing the surface roughness and surface nanotopography of (A) uncoated control discs, (B) discs coated with nHA, (C) discs coated with mHA, (D) anodised discs, (E) anodised discs coated with nHA, (F) anodised discs coated with mHA, (G) silver plated discs, (H) silver plated discs coated with nHA and (I) silver plated discs coated with mHA. Images were acquired by an Olympus LEXT OLS 3000 confocal laser scanning microscope equipped with a 408 nm LD class 2 laser (magnification: 50×; optical zoom: 1×).

Table 2. Total silver, titanium, phosphorous and calcium concentrations in the media indicating the extent of material loss from the discs and the nanocoatings due to dissolution or degradation.

	External media (physiological saline after 24 h exposure)				Sonicated media (0.85% NaCl after 60 s sonication)			
	Ag (mg l^{-1})	Ti (mg l^{-1})	P (mg l^{-1})	Ca (mg l^{-1})	Ag (mg l^{-1})	Ti (mg l^{-1})	P (mg l^{-1})	Ca (mg l^{-1})
No disc	0.00 ± 0.00^{a}*	0.01 ± 0.00^{a}	104.72 ± 1.88^{a}	56.00 ± 0.87^{abc}	0.00 ± 0.00^{a}*	0.00 ± 0.00^{a}*	0.68 ± 0.08^{a}	0.58 ± 0.07^{a}
Ti	0.02 ± 0.01^{a}	0.08 ± 0.02^{b}	100.04 ± 2.20^{a}	56.10 ± 4.07^{abc}	0.01 ± 0.00^{a}*	0.00 ± 0.00^{a}*	0.89 ± 0.12^{a}	1.42 ± 0.20^{a}
Ti + nHA	0.02 ± 0.01^{a}	0.02 ± 0.00^{a}	96.14 ± 15.71^{a}	73.28 ± 19.78^{ab}	0.00 ± 0.00^{a}*	0.32 ± 0.10^{b}	20.40 ± 7.20^{b}	39.46 ± 15.17^{b}
Ti + mHA	0.01 ± 0.00^{a}*	0.02 ± 0.00^{a}	109.97 ± 7.34^{a}	78.28 ± 13.06^{a}	0.00 ± 0.00^{a}*	0.14 ± 0.10^{bc}	21.23 ± 5.42^{b}	42.10 ± 12.28^{b}
TiO_2	0.07 ± 0.02^{b}	0.02 ± 0.00^{a}	96.82 ± 1.84^{a}	34.27 ± 0.60^{abc}	0.01 ± 0.00^{a}*	0.01 ± 0.02^{a}	0.25 ± 0.03^{a}	0.77 ± 0.10^{a}
TiO_2+nHA	0.06 ± 0.01^{ab}	0.01 ± 0.00^{a}	109.71 ± 6.12^{a}	28.82 ± 2.76^{abc}	0.01 ± 0.00^{a}*	0.05 ± 0.02^{acd}	3.30 ± 0.45^{a}	5.58 ± 0.53^{a}
TiO_2+mHA	0.05 ± 0.01^{ab}	0.02 ± 0.00^{a}	100.87 ± 4.14^{a}	28.08 ± 2.64^{bc}	0.01 ± 0.00^{a}*	0.25 ± 0.11^{bd}	3.86 ± 0.54^{a}	7.21 ± 1.06^{a}
Ag	0.16 ± 0.01^{c}	0.03 ± 0.00^{a}	91.56 ± 0.54^{a}	37.79 ± 3.91^{abc}	0.83 ± 0.05^{b}	0.00 ± 0.00^{a}*	0.48 ± 0.09^{a}	1.40 ± 0.28^{a}
Ag + nHA	0.34 ± 0.01^{d}	0.01 ± 0.00^{a}	89.95 ± 1.57^{a}	17.51 ± 0.70^{c}	1.05 ± 0.13^{c}	0.17 ± 0.05^{bd}	21.94 ± 5.29^{b}	33.43 ± 6.70^{ab}
Ag + mHA	0.32 ± 0.01^{d}	0.01 ± 0.00^{a}	94.84 ± 1.65^{a}	24.07 ± 1.13^{c}	0.13 ± 0.03^{a}	0.10 ± 0.02^{bd}	14.91 ± 2.61^{ab}	28.18 ± 5.43^{ab}

Data are means ± SEM ($n = 6$) values of total elemental concentrations measured by ICP-MS. Different letters indicate significant differences between the test groups for each chemical element (one-way ANOVA, $p < 0.05$).
*Values are below the detection limit of the ICP-MS instrument for Ag (0.012 mg l^{-1}) and Ti (0.003 mg l^{-1}).

presence of the nHA and mHA coatings on the Ti6Al4V discs was found to further encourage bacterial adhesion by 30% ($p < 0.05$).

The viability of bacteria adhered on the uncoated controls and anodised discs was very similar (57 and 64%, respectively). Application of the mHA coating to the anodised discs had no effect on the bacteria viability (62%), whereas application of the nHA coating resulted in higher viability (75%) but the increase was not statistically significant ($p > 0.05$). However, viability of bacteria adhered on the Ti + nHA and Ti + mHA discs was 97 and 102%, respectively, a 40% increase compared to the uncoated controls ($p < 0.001$). No viable bacteria were identified for any of the silver plated discs confirming the strong antibiofilm activity of the Ag, Ag + nHA and Ag + mHA discs (Figure 3(D)).

The lactate production measurements after incubation in a rich broth media for 16 h showed no evidence of biofilm inhibition on the surface of the Ti, Ti + nHA, Ti + mHA, TiO_2, TiO_2+nHA and TiO_2+mHA discs (Figure 3(F)). The lactate concentration corresponding to those groups ranged from 13.22 to 14.88 mM, which was at similar levels with the uncoated controls (14.61 ± 0.09 mM; $p > 0.05$). In contrast, no lactate was detected in the media corresponding to the Ag + nHA discs, in agreement with the low adhesion and 100% mortality results. The lactate produced by *S. sanguinis* adhered on the disc surfaces of the remaining silver plated groups (Ag and Ag + mHA discs) was limited (0.47 ± 0.33 and 1.84 ± 0.53 mM, respectively).

Discussion

This study prepared novel composite nanocoatings on titanium alloy implants consisting of biocompatible forms of HA, supplemented with nano-silver to enhance the antibacterial properties of the surface against *S. sanguinis*. The main findings were that all three silver plated groups (Ag, Ag + nHA, Ag + mHA) showed a strong antibacterial and antibiofilm activity, with the silver plated discs coated with nHA (Ag + nHA) performing best. Overall, the uncoated and anodised groups were not as effective and had little antibacterial activity and no antibiofilm potential.

Stability of the nanocoatings

A prerequisite for the successful application of a particulate coating to an implant surface is an even coverage and continuous layer of particles that bind firmly to the surface. Electron microscopy analysis showed that coatings consisted of particles ordered in a closed-packed arrangement fully covering the appropriate disc surface (Figure 1). The silver plating method formed an evenly distributed layer of nanocrystalline silver with individual particles between 25 and 50 nm in diameter (Figure 1(G)). This is similar to that reported by Lin et al. (2011), who found that silver plating also resulted in an even layer of silver particles of 25 nm or less. The deposition and sintering technique used here for applying the two HA coatings was also successful, as shown by multilayered nHA or mHA coatings on the surface of the discs (Figures 1 and 2). However, this method had a limitation in the case of the nHA coatings as some cracking was observed (Figure 2(B,E,H)). The thermal expansion coefficient of HA is 14.0×10^{-6} K^{-1}, whereas the corresponding values for Ti and TiO_2 are 8.5×10^{-6} K^{-1} and 9.19×10^{-6} K^{-1}, respectively. The cracking likely occurred due to a thermal expansion mismatch between the nanocoating and the metal substrate, which generates stress at the coating–metal interface (Chen et al., 2007). The cracks only appeared on discs coated with nHA particles, not the mHA (Figure 2), probably because nHA has a higher surface energy. Subsequently during the drying step of the coating process, shrinkage of the coating may cause some cracking (Mahé et al., 2008). For mHA particles, the cohesion between the particles and substrate is weaker allowing the particles to form clusters while the water molecules escape. Regardless, any cracks on the nHA surface did not interfere with the antimicrobial performance of the discs (see below).

The addition of the novel coatings appeared to have no appreciable effect on the quality of the underlying Ti alloy substrate. Ti6Al4V implants are highly inert and with very low metal releases in most biological media (Okazaki & Gotoh, 2005). The current study also showed low Ti metal releases after 24 h in physiological saline (<80 μg l^{-1} from uncoated discs, <20 μg l^{-1} from the anodised discs; Table 2). Notably, the titanium ion release from the Ti + nHA and Ti + mHA specimens was significantly lower compared to the uncoated controls, probably because the HA coatings acted as a physical barrier to Ti dissolution. The absence of elevated concentrations of P or Ca in the media (Table 2) is consistent with no appreciable dissolution of the HA coatings. Smolen et al. (2012) also reported very low solubility of nHA in Tris–HCl buffer. Instead, a decrease in the calcium concentration was measured in the media hosting the discs from the anodised and silver plated groups (Table 2). This could be explained by binding of the available free media calcium ions to the disc surfaces and/or the bacteria (Venegas et al., 2006).

The silver release from all three silver plated groups was very small in physiological saline (material loss was less than 0.07%; Table 2). Stebounova et al. (2011) have also reported that Ag NPs experience very low dissolution in body fluids (<0.6%).

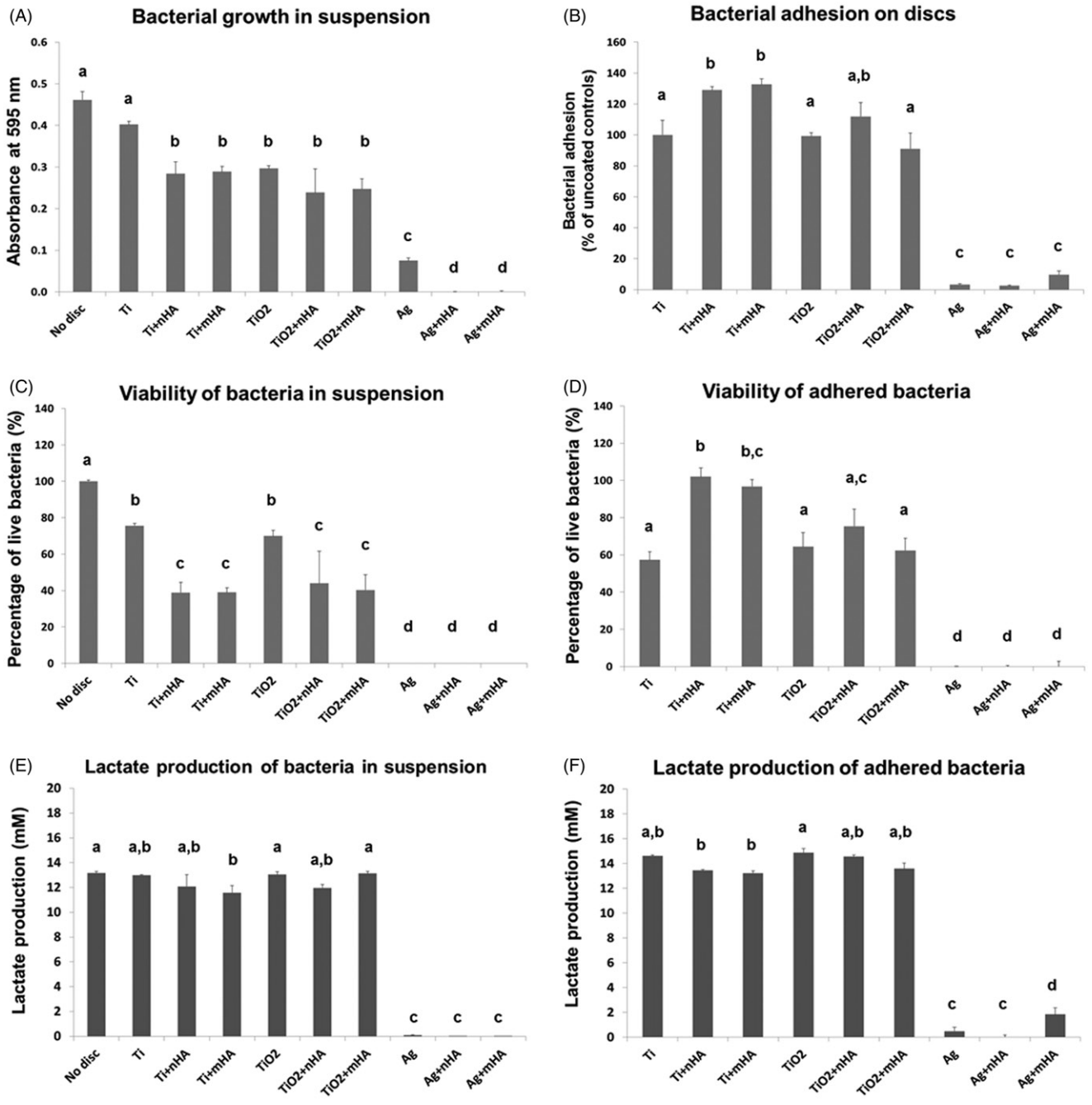

Figure 3. (A) Bacterial growth of *S. sanguinis* in suspension, measured as absorbance values of the inoculated physiological saline-BHI media recorded after a 24 h exposure to the test Ti6Al4V discs compared to the uncoated discs (Ti) and blanks (no disc), (B) the absorbance values recorded for each test group after 16 h of incubation were compared to the mean value of the uncoated controls (equated to 100% of bacterial adhesion) to give a relative measurement of bacterial adhesion, (C) percentage of live *S. sanguinis* after a 24 h exposure to coated Ti6Al4V discs compared to uncoated controls and blanks, (D) percentage of live *S. sanguinis* after incubation of the bacteria, previously adhered to the different test coatings, in fresh BHI media for 16 h, (E) total lactate production of *S. sanguinis* after a 24 h exposure to coated Ti6Al4V discs compared to uncoated controls and blanks, (F) total lactate produced by *S. sanguinis* after incubation of the bacteria, previously adhered to the different test coatings, in fresh BHI media for 16 h. Different letters indicate significant differences between the test groups (one-way ANOVA, $p < 0.05$). Note that the axis units in panels A and B are different.

Noda et al. (2009) also showed low silver release from Ag + HA coated titanium implants (260 μg l^{-1} after 24 h in foetal bovine serum), very similar to the 320–340 μg l^{-1} measured in the current study. The silver release from the Ag + nHA and Ag + mHA discs remained at μg l^{-1} levels, but was higher than that of the Ag discs (Table 2). This could be due to reaction of reduced silver with the hydroxyl groups of HA to form silver oxide, which is more soluble (0.2 mg l^{-1} in water at 25 °C). It is also possible that some silver phosphate formed during the sintering steps, and this compound is more prone to dissolution (Shirkhanzadeh & Azadegan, 1998).

The method used to collect the biofilm for counting and biochemical analysis included sonication of the discs for 60 s. The sonication was intended to detach the biofilm and is much less aggressive than the ultrasonic cleaning methods routinely used in the industry to remove surface contaminants after manufacture. Sonication processes, no matter how mild, might arguably risk damaging nanocoatings. However, the nanocoatings in this study were resilient and their integrity was largely unaffected after 60 s of sonication (Table 2), suggesting good adherence of the NPs to the titanium surfaces or the underlying nanocoatings.

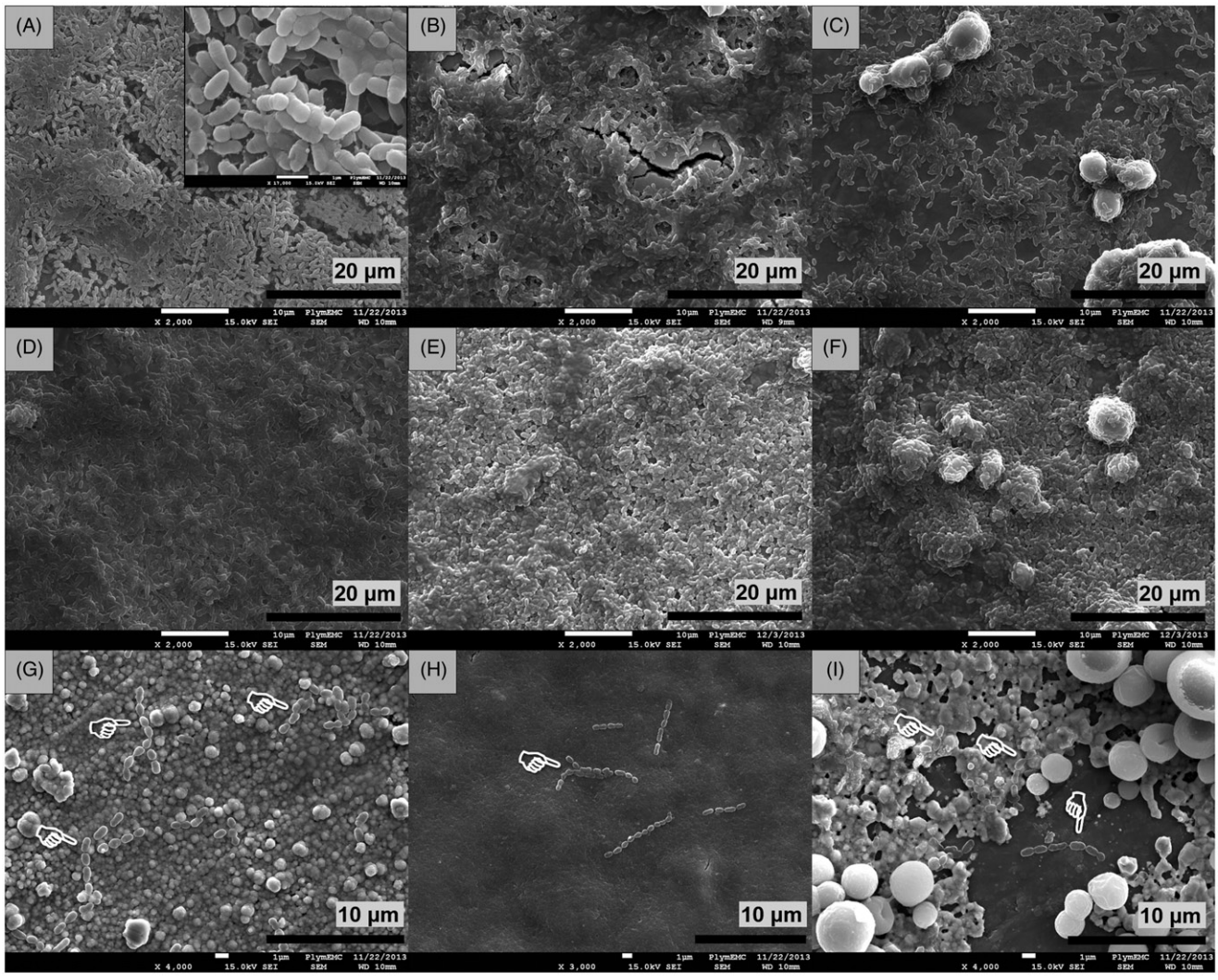

Figure 4. Scanning electron micrographs of Ti6Al4V discs after 24 h of incubation in inoculated media showing (A) formation of *S. sanguinis* biofilm on uncoated control discs (×2.0k), (B) biofilm formation on discs coated with nHA (×2.0k), (C) biofilm formation on discs coated with mHA (×2.0k), (D) biofilm development on anodised discs (×2.0k), (E) biofilm development on anodised discs coated with nHA (×2.0k), (F) biofilm development on anodised discs coated with mHA (×2.0k), (G) biofilm inhibition on silver plated discs (×4.0k), (H) biofilm inhibition on silver plated discs coated with nHA (×3.0k) and (I) biofilm inhibition on silver plated discs coated with mHA (×4.0k). White pointers indicate the locations of limited bacteria found adhered on the surfaces of silver plated groups.

For example, there was limited silver release from the silver plated discs as a result of sonication (<0.23% of total silver from the coating). Although nHA and mHA coatings did not dissolve, sonication caused partial dislodgment of the HA particles from the surfaces that resulted in some material loss (1.2–7%). However, this loss is small and would not affect the mechanical performance of the implant and is certainly outweighed by the potential clinical benefits of the HA coating.

Antibacterial effect

All the bioassays showed that the three silver plated groups were highly antibacterial causing 100% mortality to the bacteria suspended in the media (Figure 3(C)). Silver NPs and silver ions have long been known for their antimicrobial activity against oral pathogens (Allaker, 2010; Besinis et al., 2014a). However, silver with coatings of HA is not well studied. A complete bacterial growth inhibition was achieved by the Ag + nHA and Ag + mHA discs, whereas some growth was measured in the media hosting the Ag discs (Figure 3(A)). This could be attributed to a small but effective slow release of Ag from the Ag + nHA and Ag + mHA discs compared to the Ag discs (Table 2). Besinis et al. (2014b) also found some silver release in the surrounding media from a silver nanocoating applied to dentine (rich in natural HA). This caused complete growth inhibition of *Streptococci* at 0.50 mg l^{-1} of Ag, and is very similar to the inhibitory concentration reported here (0.32 mg l^{-1}, Table 2). Interestingly, in catalysis, TiO_2 doped with silver in the presence of HA has much higher photocatalytic activity than TiO_2–Ag mixtures alone, resulting in the generation of free radicals (Liu et al., 2010). Thus some cell death could be due to oxidative stress here. However, direct free Ag^+ ion toxicity derived from the external saline media is unlikely (see Besinis et al., 2014a,b) with insoluble silver chloride formation from the NaCl and milligrams amounts of proteinaceous material from the diluted broth to chelate the free metal ions. Direct contact toxicity with local Ag^+ ion release in the microenvironment on the surface of the microbes has been suggested as an alternative mechanism (Besinis et al., 2014a; Reidy et al., 2013).

The remaining test groups (no added Ag) had no measurable antibacterial activity as shown by the total lactate production results at the end of the 24 h incubation period (Figure 3(E)). However, some antibacterial activity of the Ti + nHA, Ti + mHA, TiO_2+nHA and TiO_2+mHA discs was suggested by the growth and Live/Dead assay results (Figure 3(A,C)). This finding may be an

artefact as a result of the increased surface roughness (see below) which is known to encourage bacterial adhesion (Bürgers et al., 2010). Consequently, a high number of healthy bacteria would adhere to those surfaces, and subsequently be removed from the wells together with the discs as the latter was required for the assessment of the biofilm development. Therefore, a lower proportion of healthy bacteria remained in suspension which appeared as antibacterial activity.

Antibiofilm activity and surface roughness

In the oral cavity, the surface roughness is one of the most fundamental factors affecting bacterial adhesion with rougher surfaces known to encourage biofilm formation (Quirynen et al., 2002; Teughels et al., 2006). This can be explained by favourable bacteria adhesion at locations where the microbes are protected from shear forces, thus allowing the necessary time for irreversible attachment. The effective surface area available for bacteria adhesion can also rise two- or three-fold when surface roughness increases (Teughels et al., 2006). Smooth surfaces are therefore desirable for preventing bacterial adhesion. An Ra value of 0.2 μm is considered to be the threshold surface roughness below which bacterial adhesion cannot be reduced further (Bollen et al., 1997). However, there is a dilemma for medical implants; a moderate roughness of 1–2 μm is necessary for good osseointegration and is a prerequisite for the long-term success of the implant (Albrektsson & Wennerberg, 2004).

The uncoated Ti6Al4V control discs were smooth with an Ra value of 0.358 ± 0.011 μm, and in agreement with previous reports for Grade 5 titanium alloy implants (0.30–0.50 μm, Wu et al., 2015). Although the chemistry and the nanotopography of the disc surfaces changed as a result of the anodisation and silver plating processes (Figure 1), the surface roughness values were no different to the uncoated controls (Table 1). Anodised surfaces had no effect on bacterial adhesion with results showing the formation of a fully developed biofilm (Figure 4(D)) with no clear antibiofilm properties (Figure 3(B,D,F)).

Application of an HA coating to the surface of titanium implants did increase the surface roughness (Figure 2; Table 1), and this is expected (Le Guéhennec et al., 2007; Quirynen et al., 2007). Application of the nHA coatings resulted in a surface roughness up to three-fold higher compared to the uncoated controls and the mHA coating resulted in even rougher surfaces (Figure 2; Table 1). Rougher discs were found to promote biofilm formation (Figure 3(B,D)). Bürgers et al. (2010) also found that rougher titanium implant surfaces enhance bacterial adhesion *in vitro* and *in vivo*. However, in the present study this was completely offset by the antibacterial properties of Ag when this was also added to the coating by electroplating.

Conclusions

In conclusion, the application of a dual layered silver + nHA coating renders the surface of titanium alloy implants highly antibacterial towards the oral pathogen, *S. sanguinis*; causing bacterial growth inhibition in the surrounding media and also preventing biofilm formation on the implant surface. The nanocoatings were stable and maintained their integrity in the experimental conditions used here. Critically, the silver was effective in the presence of clinically relevant forms of HA. In terms of clinical safety and regulatory approval, this study demonstrates that the novel dual layered composite used here is more effective at preventing bacterial growth than the traditional materials used for titanium implants. For the patient, this potentially offers a lowered infection risk without compromising the biocompatible HA surface required for successful osseointegration and accelerated bone healing.

Acknowledgements

We thank Sanna Hadi for her contribution to pilot studies, specimen preparation and experimental work as part of her Research Masters (ResM) degree at the University of Plymouth. Technical support from M. Emery for preparing microbial cultures is also gratefully acknowledged.

Disclosure statement

The authors report no conflicts of interest. The authors alone are responsible for the content and writing of the paper.

References

Albrektsson T, Wennerberg A. 2004. Oral implant surfaces: Part 1. Review focusing on topographic and chemical properties of different surfaces and in vivo responses to them. Int J Prosthodont 17:536–43.

Allaker RP. 2010. The use of nanoparticles to control oral biofilm formation. J Dent Res 89:1175–86.

Alt V, Bitschnau A, Österling J, Sewing A, Meyer C, Kraus R, et al. 2006. The effects of combined gentamicin–hydroxyapatite coating for cementless joint prostheses on the reduction of infection rates in a rabbit infection prophylaxis model. Biomaterials 27:4627–34.

Besinis A, De Peralta T, Handy RD. 2014a. The antibacterial effects of silver, titanium dioxide and silica dioxide nanoparticles compared to the dental disinfectant chlorhexidine on *Streptococcus mutans* using a suite of bioassays. Nanotoxicology 8:1–16.

Besinis A, De Peralta T, Handy RD. 2014b. Inhibition of biofilm formation and antibacterial properties of a silver nano-coating on human dentine. Nanotoxicology 8:745–54.

Besinis A, De Peralta T, Tredwin CJ, Handy RD. 2015. Review of nanomaterials in dentistry: interactions with the oral microenvironment, clinical applications, hazards, and benefits. ACS Nano 9:2255–89.

Bollen CM, Lambrechts P, Quirynen M. 1997. Comparison of surface roughness of oral hard materials to the threshold surface roughness for bacterial plaque retention: a review of the literature. Dent Mater 13:258–69.

Bürgers R, Gerlach T, Hahnel S, Schwarz F, Handel G, Gosau M. 2010. In vivo and in vitro biofilm formation on two different titanium implant surfaces. Clin Oral Implants Res 21:156–64.

Chen F, Lam WM, Lin CJ, Qiu GX, Wu ZH, Luk KDK, et al. 2007. Biocompatibility of electrophoretical deposition of nanostructured hydroxyapatite coating on roughen titanium surface: in vitro evaluation using mesenchymal stem cells. J Biomed Mater Res B 82:183–91.

Dunne WM. 2002. Bacterial adhesion: seen any good biofilms lately? Clin Microbiol Rev 15:155–66.

Figueiredo M, Henriques J, Martins G, Guerra F, Judas F, Figueiredo H. 2010. Physicochemical characterization of biomaterials commonly used in dentistry as bone substitutes—comparison with human bone. J Biomed Mater Res B 92:409–19.

Gutmann I, Wahlefeld AW. 1974. l-(+)-Lactate determination with lactate dehydrogenase and NAD. In: Bergmeyer HU, ed. Methods in Enzymatic Analysis. London: Academic Press, 1464–8.

He G, Wu Y, Zhang Y, Zhu Y, Liu Y, Li N, et al. 2015. Addition of Zn to the ternary Mg–Ca–Sr alloys significantly improves their antibacterial properties. J Mater Chem B 3:6676–89.

Hirakawa K, Mori M, Yoshida M, Oikawa S, Kawanishi S. 2004. Photo-irradiated titanium dioxide catalyzes site specific DNA damage via generation of hydrogen peroxide. Free Radic Res 38:439–47.

Kim JS, Kuk E, Yu KN, Kim JH, Park SJ, Lee HJ, et al. 2007. Antimicrobial effects of silver nanoparticles. Nanomedicine 3:95–101.

Kozlovsky A, Artzi Z, Moses O, Kamin-Belsky N, Greenstein RBN. 2006. Interaction of chlorhexidine with smooth and rough types of titanium surfaces. J Periodontol 77:1194–200.

Le Guéhennec L, Soueidan A, Layrolle P, Amouriq Y. 2007. Surface treatments of titanium dental implants for rapid osseointegration. Dent Mater 23:844–54.

Lessa FC, Aranha AM, Nogueira I, Giro EM, Hebling J, Costa CA. 2010. Toxicity of chlorhexidine on odontoblast-like cells. J Appl Oral Sci 18:50–8.

Lin WP, Wesolowski DE, Lee CC. 2011. Barrier/bonding layers on bismuth telluride (Bi_2Te_3) for high temperature thermoelectric modules. J Mater Sci-Mater Electron 22:1313–20.

Liu Y, Liu CY, Wei JH, Xiong R, Pan CX, Shi J. 2010. Enhanced adsorption and visible-light-induced photocatalytic activity of hydroxyapatite modified Ag–TiO_2 powders. Appl Surf Sci 256:6390–4.

Mahé M, Heintz JM, Rödel J, Reynders P. 2008. Cracking of titania nanocrystalline coatings. J Eur Ceram Soc 28:2003–10.

Mishra SK, Teotia AK, Kumar A, Kannan S. 2016. Mechanically tuned nanocomposite coating on titanium metal with integrated properties of biofilm inhibition, cell proliferation, and sustained drug delivery. Nanomed Nanotechnol Biol Med 13:23–35.

Morones JR, Elechiguerra JL, Camacho A, Holt K, Kouri JB, Ramirez JT, et al. 2005. The bactericidal effect of silver nanoparticles. Nanotechnology 16:2346–53.

Moy PK, Medina D, Shetty V, Aghaloo TL. 2005. Dental implant failure rates and associated risk factors. Int J Oral Maxillofac Implants 20:569–77.

Noda I, Miyaji F, Ando Y, Miyamoto H, Shimazaki T, Yonekura Y, et al. 2009. Development of novel thermal sprayed antibacterial coating and evaluation of release properties of silver ions. J Biomed Mater Res B 89:456–65.

Norowski PA, Bumgardner JD. 2009. Biomaterial and antibiotic strategies for peri-implantitis: a review. J Biomed Mater Res B Appl Biomater 88:530–43.

Okazaki Y, Gotoh E. 2005. Comparison of metal release from various metallic biomaterials in vitro. Biomaterials 26:11–21.

Paquette DW, Brodala N, Williams RC. 2006. Risk factors for endosseous dental implant failure. Dent Clin N Am 50:361–74.

Phillips MJ, Darr JA, Luklinska ZB, Rehman I. 2003. Synthesis and characterization of nano-biomaterials with potential osteological applications. J Mater Sci Mater Med 14:875–82.

Pucher JJ, Daniel C. 1992. The effects of chlorhexidine digluconate on human fibroblasts in vitro. J Periodontol 63:526–32.

Quirynen M, Abarca M, Van Assche N, Nevins M, Van Steenberghe D. 2007. Impact of supportive periodontal therapy and implant surface roughness on implant outcome in patients with a history of periodontitis. J Clin Periodontol 34:805–15.

Quirynen M, De Soete M, Van Steenberghe D. 2002. Infectious risks for oral implants: a review of the literature. Clin Oral Implants Res 13:1–19.

Radin S, Campbell JT, Ducheyne P, Cuckler JM. 1997. Calcium phosphate ceramic coatings as carriers of vancomycin. Biomaterials 18:777–82.

Reidy B, Haase A, Luch A, Dawson KA, Lynch I. 2013. Mechanisms of silver nanoparticle release, transformation and toxicity: a critical review of current knowledge and recommendations for future studies and applications. Materials 6:2295–350.

Seuss S, Heinloth M, Boccaccini AR. 2016. Development of bioactive composite coatings based on combination of PEEK, bioactive glass and Ag nanoparticles with antibacterial properties. Surf Coat Tech 301:100–5.

Shirkhanzadeh M, Azadegan M. 1998. Formation of carbonate apatite on calcium phosphate coatings containing silver ions. J Mater Sci Mater Med 9:385–91.

Sieh R, Le HR, Cree AM. 2015. Process optimisation of non-cyanide Ag-PTFE metal matrix composite electroplating for threaded connections. Trans IMF 93:232–40.

Smolen D, Chudoba T, Gierlotka S, Kedzierska A, Lojkowski W, Sobczak K, et al. 2012. Hydroxyapatite nanopowder synthesis with a programmed resorption rate. J Nanomater. 2012;9:Article ID 841971.

Stebounova LV, Adamcakova-Dodd A, Kim JS, Park H, O'Shaughnessy PT, Grassian VH, Thorne PS. 2011. Nanosilver induces minimal lung toxicity or inflammation in a subacute murine inhalation model. Part Fibre Toxicol 8:5–17.

Svanborg LM, Hoffman M, Andersson M, Currie F, Kjellin P, Wennerberg A. 2011. The effect of hydroxyapatite nanocrystals on early bone formation surrounding dental implants. Int J Oral Maxillofac Surg 40:308–15.

Teughels W, Van Asshe N, Sliepen I, Quirynen M. 2006. Effect of material characteristics and/or surface topography on biofilm development. Clin Oral Implan Res 17:68–81.

Vargas-Reus MA, Memarzadeh K, Huang J, Ren GG, Allaker RP. 2012. Antimicrobial activity of nanoparticulate metal oxides against peri-implantitis pathogens. Int J Antimicrob Agents 40:135–9.

Venegas SC, Palacios JM, Apella MC, Morando PJ, Blesa MA. 2006. Calcium modulates interactions between bacteria and hydroxyapatite. J Dent Res 85:1124–8.

We M, Ruys AJ, Swain MV, Milthorpe BK, Sorrell CC. 2005. Hydroxyapatite-coated metals: interfacial reactions during sintering. J Mater Sci Mater Med 16:101–6.

Williams DF. 1977. Titanium as a metal for implantation. Part 2: Biological properties and clinical applications. J Med Eng Technol 1:266–70.

Wong MS, Chu WC, Sun DS, Huang HS, Chen JH, Tsai PJ, et al. 2006. Visible-light-induced bactericidal activity of a nitrogen-doped titanium photocatalyst against human pathogens. Appl Environ Microbiol 72:6111–16.

Wu C, Chen M, Zheng T, Yang X. 2015. Effect of surface roughness on the initial response of MC3T3-E1 cells cultured on polished titanium alloy. Bio-Med Mater Eng 26:155–64.

Yang GL, He FM, Hu JA, Wang XX, Zhao SF. 2009. Effects of biomimetically and electrochemically deposited nano-hydroxyapatite coatings on osseointegration of porous titanium implants. Oral Surg Oral Med Oral Pathol 107:782–9.

Zhao L, Chu PK, Zhang Y, Wu Z. 2009. Antibacterial coatings on titanium implants. J Biomed Mater Res Part B Appl Biomater 91:470–80.